Korean J. Chem. Eng., 37(11), 1859-1866 (2020)
DOI: 10.1007/s11814-020-0609-z

pISSN: 0256-1115
eISSN: 1975-7220

Experimental study of gas-liquid two-phase bubbly flow characteristics in a static mixer with three twisted leaves

Huibo Meng*, Yuning Hao*, Yanfang Yu*,†, Zhonggen Li*, Shuning Song, and Jianhua Wu***

*Liaoning Key Laboratory of Chemical Technology for Efficient Mixing, Shenyang University of Chemical Technology, Shenyang 110142, P. R. China
**School of Chemistry and Molecular Bioscience, The University of Queensland, Brisbane 4067, Australia
(*Received 17 March 2020 • Revised 15 May 2020 • Accepted 8 June 2020*)

Abstract−Under the conditions of liquid phase inlet Re ranging from 9,836 to 56,206 and gas fraction α from 4.76% to 66.67%, gas-liquid two-phase bubbly flow was investigated in a static mixer with three twisted leaves (TKSM) with a diameter of 100 mm and an aspect ratio of 1.5. A high-speed camera Revealer-2F04M with a resolution of 1,920×1,080 pixels was used to capture the evolution of bubble groups at the different axial windows of mixer elements. The results show that the flow pattern in the TKSM is still in bubbly flow at the flow rate of continuous phase Q_L no more than 1.0 m^3/h and gas fraction α higher up to 54.55%-66.67%. The Sauter mean diameter d_{32} of bubble groups gradually decreased with the increase of the mixing elements number. With the given liquid flow rate $Q_L \leq 1.0$ m^3/h, the Sauter mean diameter d_{32} firstly decreased and then increased with the increase of gas flow rate. The local minimum of d_{32} was obtained at Q_G=0.72 m^3/h and 84.5% of the d_B/D_0 is in the range of 0.02-0.05. The relationship among Sauter mean diameter, the inner diameter and the non-dimensional residence time τ satisfies the correlation $We^{0.35} \cdot d_{32}/D_0 = 0.026\tau^{-0.17}$.

Keywords: Static Mixer, Gas-liquid Two-phase, Flow Pattern, Sauter Mean Diameter, Dimensionless Residence Time

INTRODUCTION

Multiphase flow mixing widely exists in the chemical industry, pharmaceutical industry, biological science, food production and other processes. Gas-liquid two-phase flow, as a turbulent dispersed multiphase flow in which dispersed phase and continuous phase coexist, has strong turbulent interactions and its mixing is a complex phenomenon [1]. Understanding and predicting bubbly flow behavior between fluids is critical to improving production efficiency and quality [2]. Increasing the mixing efficiency of the mixer under the condition of low energy consumption is a criterion for evaluating the mixer performance [3].

Static mixers are devices equipped with specific mixing elements in a smooth tube for continuous flow and mixing applications. It has no moving parts and the fluid flow is driven by the pressure difference across the static mixer [4]. Static mixers can achieve better mixing results with less energy consumption and be employed as an alternative to replace the traditional stirred tank [5]. Bayer et al. [6] found that a 0.6 L small continuous-flow static mixer could replace a 6,000 L batch reactor to handle mixing of viscous materials with residence time and energy consumption reduced by ~15,000 and 18 times, respectively. Thakur et al. summarized the potential advantages of static mixers over conventionally agitated vessels [7].

The Kenics static mixer (KSM) employs helical Kenics elements inside the bare tube for many process intensification industries. KSM has become a standard static mixer that has been used commercially for many years. KSM consists of a series of left and right-hand helical blades which are alternatively arranged and have been given a twist angle of 90°-180° [8]. Hobbs et al. [9] numerically studied the three-dimensional chaotic mixing characteristics in the KSM. They found that the static mixer elements with twist angle of 120° produced more energy efficiency than standard KSM [10,11]. Kumar et al. [12] conducted numerical research on the pressure drop in KSM under a range of Re=1-25,000. At higher Re with a range of 10,000-25,000, the pressure drop across the KSM increased significantly. Zidouni et al. [13] numerically studied the axial and radial gas phase distribution in the KSM under different initial bubble sizes (3, 5.8 and 8 mm). The effects of Re number, Weber number and number of mixing elements on the Fanning friction were evaluated by Haddadi et al. [14], who found that the Sauter mean diameter decreased with the increasing of Weber and mixing elements number.

The KSM also plays an important role in environmental protection. Tajima et al. [15] proposed a new method for ocean sequestration of the anthropogenic CO_2 by using a KSM. They experimentally explored and analyzed the formation process of CO_2 droplets and found that the size of the CO_2 droplet formation rapidly decreased with the increase of the number of mixing elements [16]. According to arrangement of different spiral blades, MSM, KSM, SSM, RSM static mixers can be formed. Tajima et al. [17] compared the effects of these four static mixers on the disposal of CO_2 droplets and found that KSM can reduce the size of CO_2 droplets faster.

According to previous studies, some researchers have developed many new types of static mixer in recent years. Wu [18] proposed a new type of static mixer which is a single smooth tube equipped with multi-twisted leaves in the circumference; it has better disper-

†To whom correspondence should be addressed.
E-mail: taroyy@163.com

sion mixing efficiency than KSM in the process of producing propylene oxide by propylene chlorohydrination reaction. Zhang et al. [19] studied the effect of different combinations of two twisted blades on the turbulent heat transfer performance in a double twisted static mixer. They found that the effect of the dislocation angle between the two adjacent sets of twisted blades on the Nusselt number and pressure drop was significantly greater than the twist direction of elements. Meng et al. [20] conducted a numerical study on the mixing characteristics of high-viscosity fluids in the novel static mixers. The mixing efficiency of three novel static mixers was evaluated through G value, particle distribution and stretching rates. It was concluded that a static mixer with three twisted leaves (TKSM) had the strongest micro-mixing ability in the novel static mixers. However, the multiphase flow characteristics in the novel static mixer are rarely studied. To reveal the bubble flow characteristics of gas-liquid two-phase mixing process in a TKSM, an air-water two-phase experiment was conducted under the liquid Reynolds number Re=9836-56206 with average gas fractions α=4.76%-66.67% at the inlet. The distribution of bubble d_{32}, the dimensionless bubble diameter and the relationship between Weber number and residence time were used to evaluate the bubble performance in the TKSM.

PHYSICAL MODEL AND EXPERIMENT

1. The Physical Model of the Static Mixer

The physical model of the TKSM used in this experiment is shown in Fig. 1. For the classical KSM, the mixing elements consist of helical blades with a twist of 180°, and the upper and lower edges of the two adjacent groups of mixed elements are staggered by 90° with their twist directions are opposite [21-23]. The advantages of the TKSM structure are that three spiral blades with the same twist direction are uniformly fixed on the shaft core at a circumferential angle of 120° and the adjacent two mixing elements are oppositely twisted and staggered by 60° [18]. The TKSM model of this experiment has an internal diameter of 100 mm and employs 13 groups of mixing elements which are numbered from the bot-

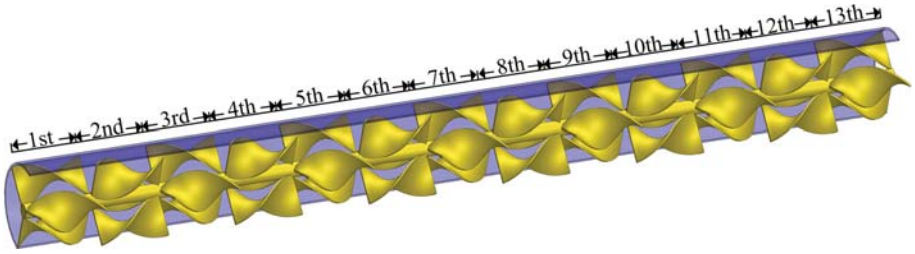

Fig. 1. The physical model of TKSM.

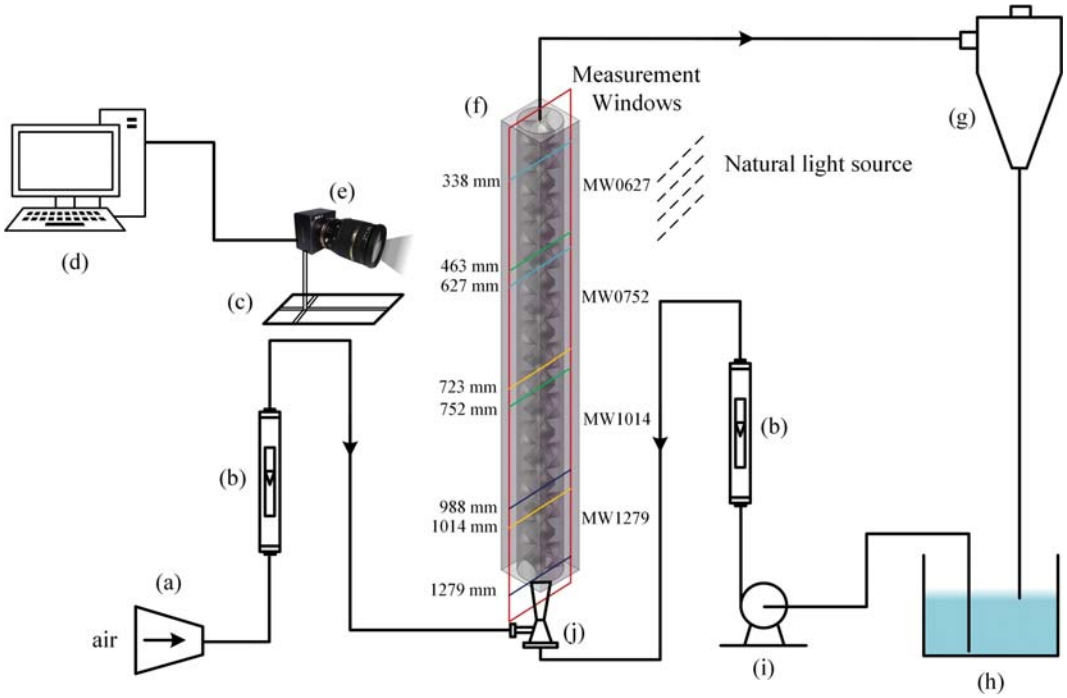

Fig. 2. Schematic layout of the gas-liquid two-phase flow experimental setup: (a) Oil-free air compressor, (b) rotor flow meter, (c) ISEL 3D synchronous coordinate traverse, (d) computer, (e) high speed camera, (f) TKSM, (g) cyclone separator, (h) water tank, (i) Wilo centrifugal pump, (j) jet pump.

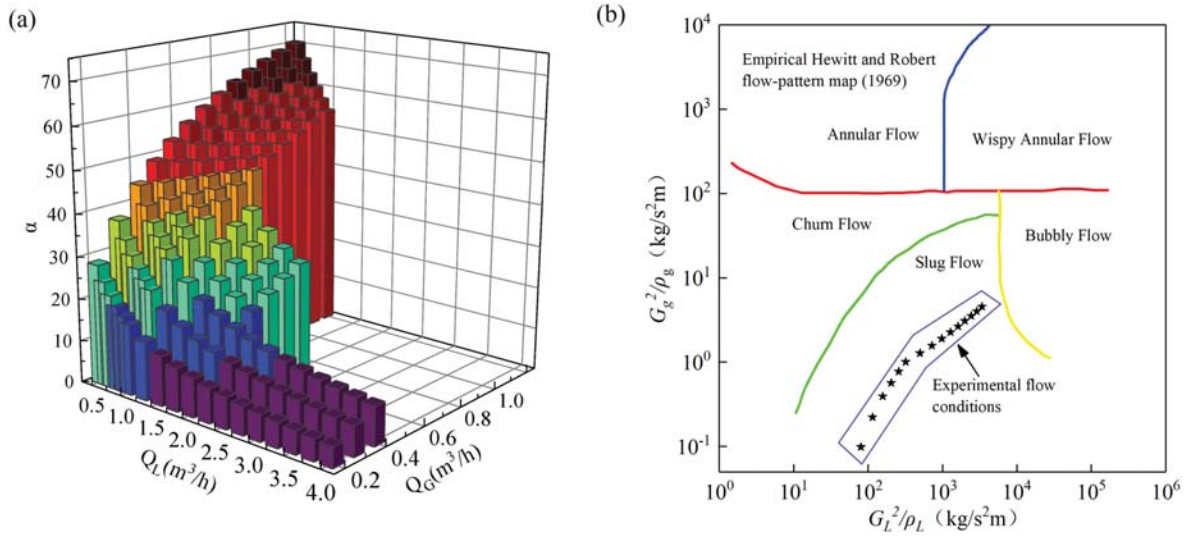

Fig. 3. The experimental operating conditions: (a) The matching relationship between the Q_G and Q_L and the corresponding gas fraction distribution and (b) the relationship between experimental conditions and empirical Hewitt and Robert's flow pattern map for vertical upward gas-liquid cocurrent flow.

tom to the top. The single spiral blades have a length of 60 mm, a width of 40 mm (aspect ratio of 1.5), and a thickness of approximately 2 mm. With the same tube length and blade thickness, the KSM employed in the experiment consists of four helical blades with a length of 180 mm and a width of 100 mm.

2. Apparatus and Experimental Procedure

A schematic layout of the gas-liquid two-phase flow experimental setup in TKSM is illustrated in Fig. 2. The air and water phases are pumped by the oil-free air compressor (SY-95/7, Zhejiang Shengyuan Compressor Manufacturing Co., Ltd.) and stainless multistage centrifugal pump (MHI802, Wilo), respectively. The two-phase working fluids encountered in the jet pump are located at the bottom of the mixer. The inner tube diameter of the jet pump for water and gas inlets is 25 mm and 14 mm, respectively. The volumetric flow rates of air and water are measured by glass rotor flowmeter (G10-15, Shenyang Beixing Instrument Co., Ltd.) and stainless rotor flowmeter (LZD-50/Y10/RR1/ESK, Shenyang Beixing Instrument Co., Ltd.). The measurement range of G10-15 and LZD-50 flowmeters, which have a 1.5 accuracy class, was 0.2-2.0 m^3/h and 1-10 m^3/h, respectively. The recycling liquid phase is separated from mixture phases by a cyclone separator after effective mixing. The mixing segments are placed in a plexiglass tube with an inner diameter of 100 mm, and a square plexiglass jacket is employed on the outside of the round tube to correct the distortion and refraction [24,25]. The bubble groups in the vertical TKSM are evaluated by a high-speed camera with 8-bit resolution and 1,920×1,080 pixel window (Revealer-2F04M, Fuhuang AgileDevice High-tech Information Technology Co., Ltd.). The measurement coordinates of Revealer-2F04M high-speed camera are controlled by 3D synchronous coordinate Traverse (234000 SDZ5835, Isel Germany AG) to capture the four axial measurement windows named MW0627, MW0752, MW1014, MW1279 from top to bottom, respectively. The sampling images with the length of time series 25640 *ms* are online imported into the Dell Inspiron 3670 computer.

RESULTS AND DISCUSSION

1. Flow Pattern Identification

The air as dispersed phase and the water as the continuous phase have an inlet flow rate range of Q_G=0.20-1.20 m^3/h and Q_L=0.50-4.00 m^3/h. Thus, the inlet Re of liquid phase ranges from 9,836 to 56,206 and the corresponding gas fraction α is in the range of 4.76% to 66.67%. Fig. 3(a) shows the matching relationship between the air and water phase and the corresponding gas fraction. This experiment is based on a vertical upward gas-liquid two-phase flow model. Due to the interaction of surface tension and gravity, the gas-liquid two-phase flow in the mixing tube generates several flow patterns which determine the mixing efficiency of the gas-liquid two phases. It can be seen in Fig. 3(b) that the same operating conditions in the smooth tube as above experiment mentioned in Fig. 3(a) are scattered in the slug flow region of the empirical Hewitt and Robert flow diagrams [26]. The horizontal and vertical coordinates represent the momentum fluxes of the liquid and gas phases, respectively, expressed by G^2/ρ (kg/s²m), where G (kg/m²s) is the mass flow rate of the gas phase and the liquid phase.

The distribution of bubble groups in the different measurement windows at lower and higher air fraction is depicted in Fig. 4 and Fig. 5, respectively. At flow rate of continuous phase Q_L higher than 1.0 m^3/h and lower gas fraction (4.72%-16.67%), the diameter distribution of the bubble groups becomes smaller and the shape is mainly spherical and cap-shaped. With the decreasing measurement height in Fig. 4, the coupled effects among splitting function, radial mixing and flow reversal have an obvious inhibition on the bubble coalescence. Furthermore, it can be clearly seen in Fig. 5 that the flow pattern in the TKSM is still in bubbly flow at flow rate of continuous phase Q_L no more than 1.0 m^3/h and the corresponding gas fraction α higher up to 54.55%-66.67%. Obviously, it the dispersion function for bubble groups is clearly enhanced by the mixing elements in the TKSM.

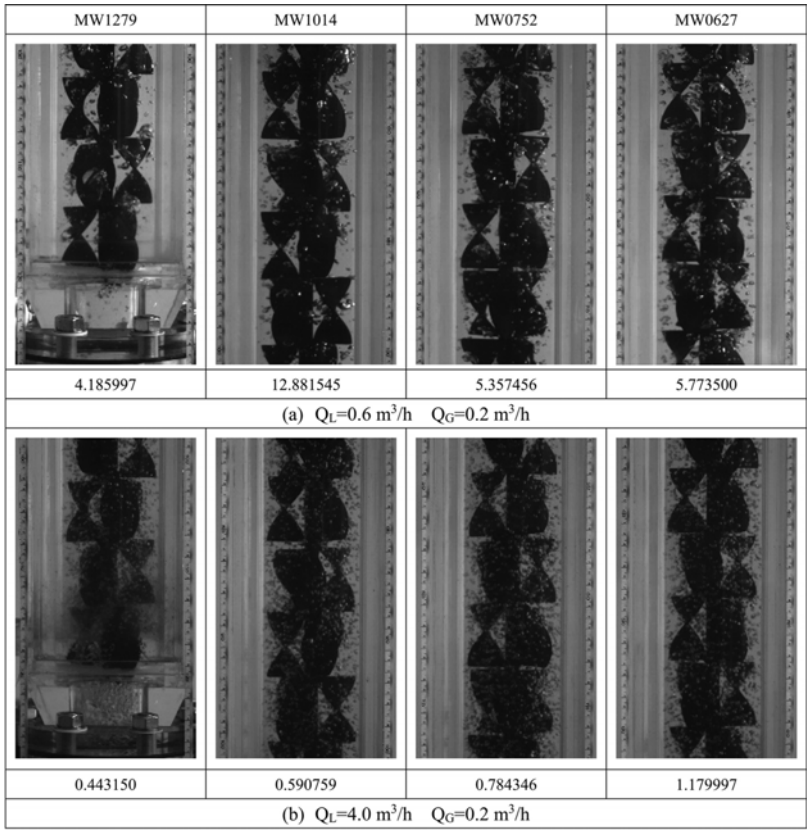

Fig. 4. The bubble group distribution in the different measurement windows of TKSM at lower air fraction (a) Q_L=0.60 m³/h and Q_G=0.20 m³/h, (b) Q_L=4.0 m³/h and Q_G=0.2 m³/h.

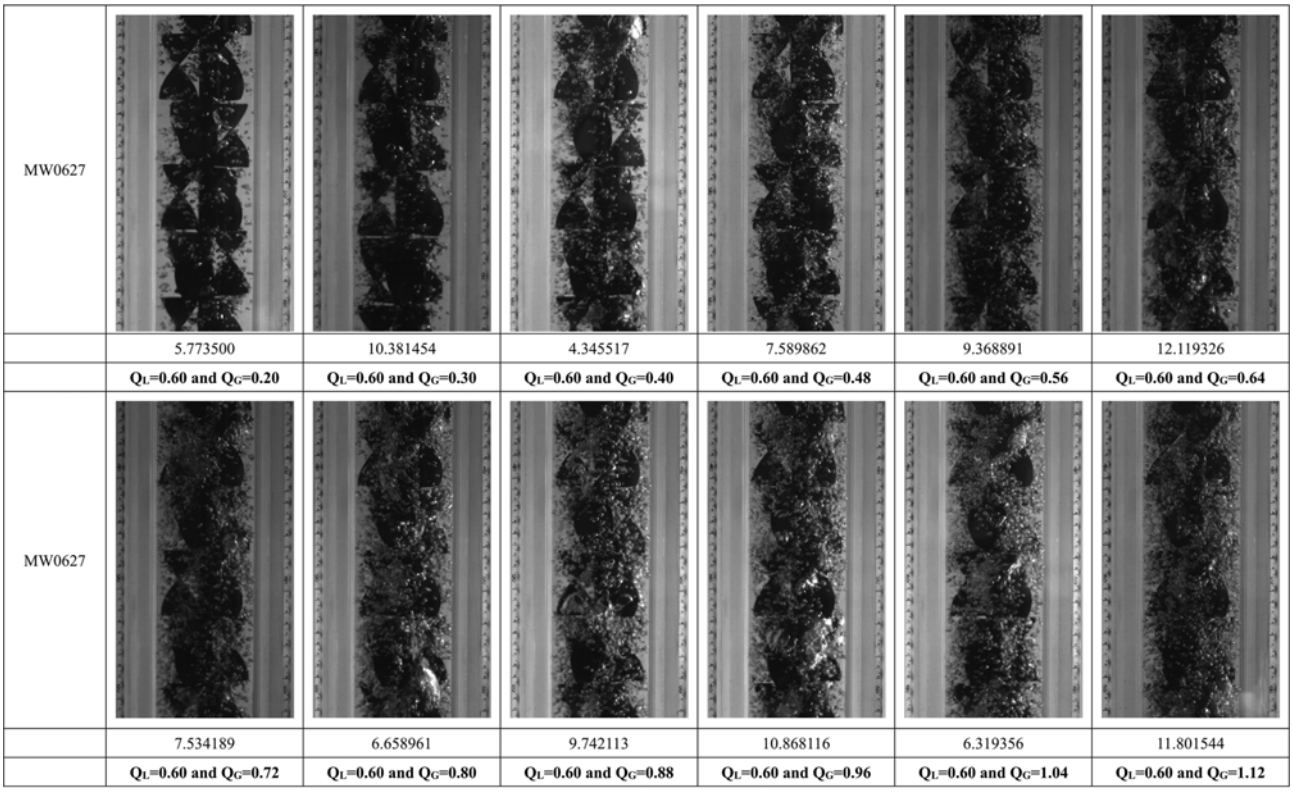

Fig. 5. The bubble group distribution at the MW0627 of TKSM versus the increasing air flow rate at Q_L=0.60 m³/h.

2. Diameter Distribution of Bubble Groups

Image Pro Plus was used to calibrate the bubble diameter in the gray pictures with an accuracy of one pixel of 152 μm×148 μm. The bubble diameter was evaluated by the average length of diameters measured at 2 degree intervals and passing through bubbles centroid. The distribution of bubble diameters can be characterized by the average diameter of the bubbles. In this study, the Sauter mean diameter (d_{32}) was used as an indicator of the bubble diameter distribution, defined as:

$$SMD = \frac{\Sigma n_i d_B^3}{\Sigma n_i d_B^2} \quad (1)$$

where, d_B and n_i represent the bubble diameter of the *i*th group and its corresponding number.

From the bottom of the mixer, each group of mixing elements was numbered and monitored, and the mean diameter of bubble groups was obtained as shown in Fig. 6. From Fig. 6(a), the bubble diameter in the TKSM obviously decreases gradually with the increase of both the number of mixing elements and liquid volume flux at the same air flow rate. For much smaller flow rate difference between the air-liquid phases, there are two tendencies for Sauter mean diameter of the bubbles in the mixer: the bubble diameter decreases at a faster rate in the first two groups of mixing elements and decreases linearly at a slower rate in the downstream mixing inserts. In Fig. 6(a), the increase of continuous phase velocity causes the overall decrease of bubble d_{32}, especially in the case of a high Reynolds number. The main reason for this phenomenon is that the bubble groups are continuously split by the downstream mixing elements in a much shorter flow time. At the same time, the shear flow field in the TKSM causes bubble fragmentation due to the instability of the larger bubble surface and the secondary flow collision [27]. On the other hand, the smaller bubbles are less likely to be aggregated between the bubbles due to their larger surface tension. Fig. 6(b) shows the probability density distribution of average bubble diameter at MW0751, MW1014 and MW1279, respectively. As the number of mixing groups increases, the peak not only moves toward the smaller diameter but also becomes much larger and narrower. The bubble diameter of different axial measurement windows exhibits a Gaussian distribution with long tails of larger bubbles. For the same tube length and operation conditions, the characteristics of bubble groups in the KSM was evaluated. In Fig. 6(c) the average bubble diameter in

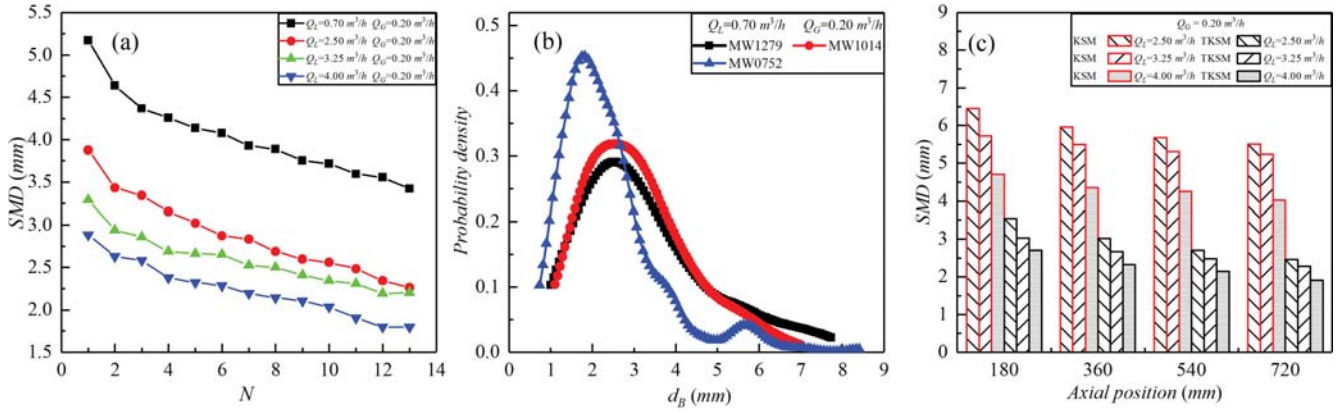

Fig. 6. The distribution profiles of bubble groups of (a) Sauter mean diameter and the number of the mixing element, (b) probability density distribution, and (c) axial profiles of Sauter mean diameter in the TKSM and KSM.

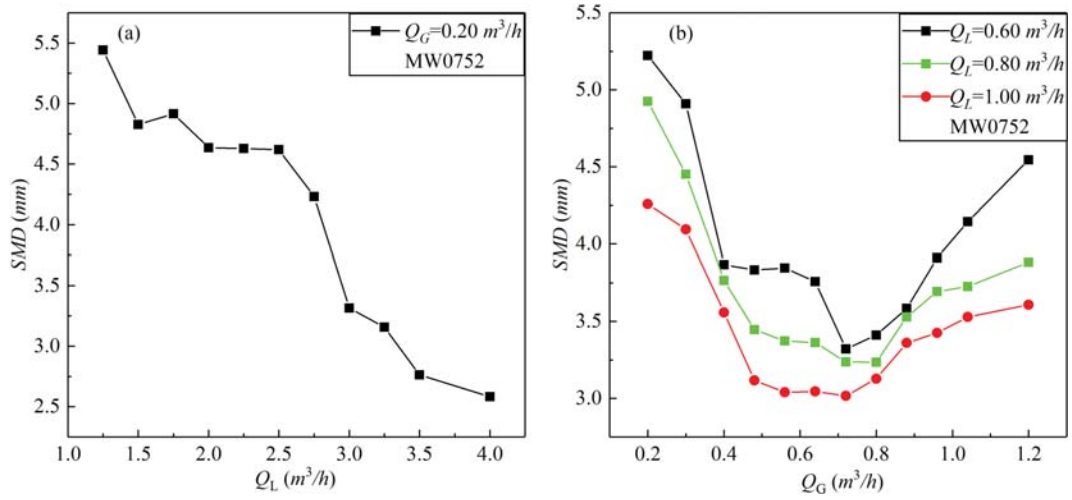

Fig. 7. The distribution of d_{32} at the MW0752 window (a) under constant gas flow rate, and (b) under constant liquid flow rate.

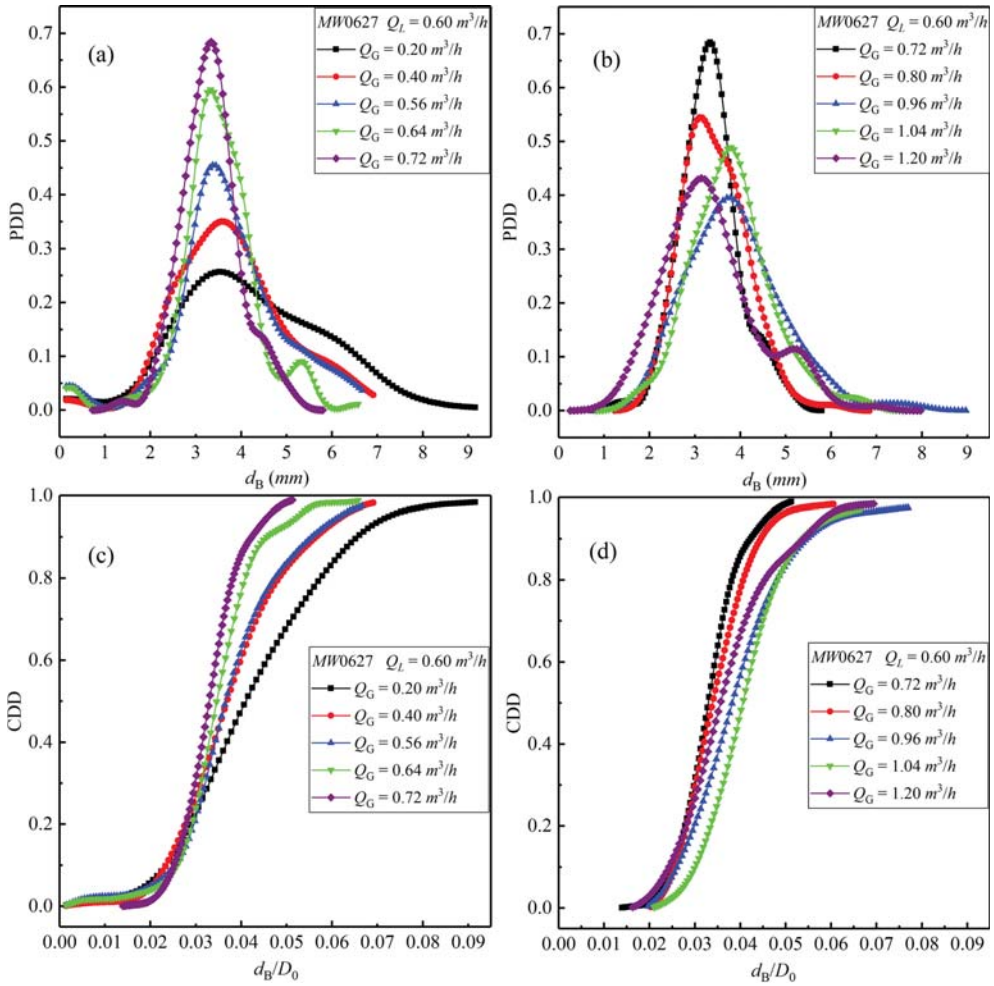

Fig. 8. Probability and cumulative density distribution of bubble mean diameter in TKSM.

the KSM decreases gradually with the increase of axial flow length and liquid flow rate at the same air volume flux. The Sauter mean diameter in the TKSM becomes much smaller by 39.94%-42.68%, 42.57%-48.71%, 38.62%-40.91% than that in the KSM for Q_L=2.50, 3.25, 4.0 m^3/h, respectively. As a result, the enhancement effect of TKSM on dispersion and breakup of bubble groups is obviously larger by 40.37%-44.10%.

In this experiment, the zero of ruler labels was set at the top of the mixer. The distribution of the bubble d_{32} in the TKSM was evaluated in Fig. 7 with the different flow rates of liquid and gas phase at the monitored windows MW0752 corresponding to the 9-10th groups of mixing elements. In Fig. 7(a) the mean Sauter diameter decreases when the liquid flow rate increases and becomes much larger than the given air flow rate. There is a nearly linear relationship and the diameter of the bubbles d_{32} can be predicted by the fitting relationship as follows: $d_{32}=-1.071Q_L+6.8$. Furthermore, in Fig. 7(b), the bubble d_{32} in the TKSM decreases when the air flow rate gradually increases from 0.2 to 0.72 m^3/h at Q_L=0.60 m^3/h. Similar profiles between d_{32} and air flow rate could be obtained for $Q_L \leq 1.0$ m^3/h. That may be induced by the increasing turbulence which plays an important role in the breakup of bubbles. However, bubble d_{32} increases when the gas flow rate increases and becomes larger than the given liquid flow rate. This indicates that the centrifugal force and bubble forces slightly improve the coalescence probability for smaller bubble groups.

Fig. 8 shows the probability and cumulative density distribution of bubble diameters in the gas phase flow Q_G=0.20-1.12 m^3/h when the liquid phase flow rate Q_L is constant at 0.6 m^3/h at the measurement window MW0627. In Fig. 8(a) the peaks of PDD shift to the left and become much higher and narrower, which indicates that the mean diameter of bubble groups gradually decreases with the increasing gas flow rate until Q_G=0.72 m^3/h. As it turns out, just the opposite in Fig. 8(b): the peaks shift to the right again and become much lower and fatter with the increasing gas flow rate Q_G=0.72-0.96 m^3/h. It may be because the increasing chance of collisions contributes to bubble coalescence. The mean bubble diameter gradually stabilizes for Q_G>1.04 m^3/h due to the increasing turbulence. In Fig. 8(c) and 8(d) the local minimum of d_{32} is obtained at Q_L=0.60 m^3/h and Q_G=0.72 m^3/h and the probability of bubble diameter d_B/D_0 less than 0.02 is 13.67% and 84.50% of the d_B/D_0 is in the range of 0.02-0.05. At Q_L=0.60 m^3/h and Q_G= 0.20 m^3/h, the probability of bubble diameter d_B/D_0 in the range of 0-0.02, 0.02-0.05 and 0.05-0.08 is 5.55%, 61.94% and 29.71%, respectively. The curves exhibit long tails on the high bubble diameter of

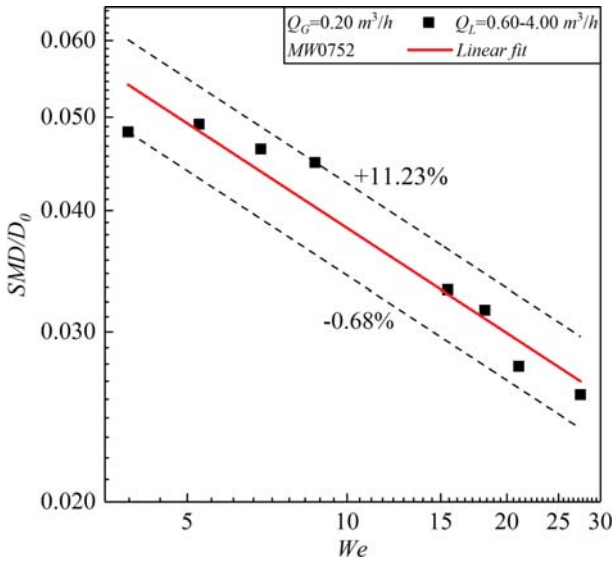

Fig. 9. The relationship between the dimensionless Sauter mean diameter and the Weber number.

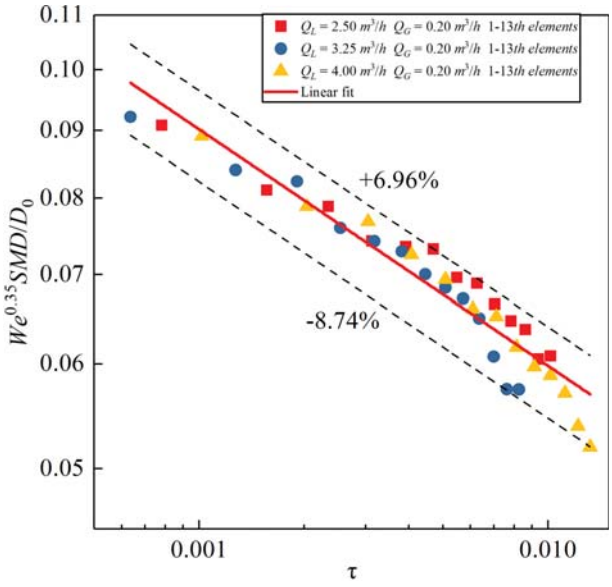

Fig. 10. Relationship between the dimensionless $(d_{32}/D_0)\times We^{0.35}$ and dimensionless residence time.

0.07-0.09, indicating that a subset of points experiences high bubble coalescence. The extended tails on the lower bubble diameter side of the curves indicate that the splitting, radial mixing and flow reversal functions play an important role in the breakup of bubble groups.

Because the diameter evolution of bubble groups is related to the Weber number, Tajima et al. [15,16] experimentally investigated the dependence of the dimensionless Sauter mean diameter of dispersed CO_2 droplets in a Kenics static mixer on the continuous phase velocity. In Fig. 9 there is a linear relationship fitted based on least square method with an acceptable deviation range of −10.68%~+11.236% between the dimensionless Sauter mean diameter of the bubble and the Weber number at the monitored window MW0752 of the TKSM. The relationship among the bubble diameter, the inner diameter of the mixer and the Weber number could be obtained as follows:

$$d_{32}/D_0=0.0879\cdot We^{-0.35} \tag{2}$$

where $We=u^2\rho D_0/\sigma$ is the Weber number of the continuous phase, ρ and u are the density and velocity of the continuous phase, respectively; σ is the surface tension.

In the mixing process of static mixers, the degree of mixing is not only dependent on the inlet flow rate but also on the residence time of the mixture in the mixer. Nevertheless, it does not contain enough information about the residence time in Eq. (2). According to the previous experimental results [16], the diameter of the bubble depends on the number of mixing elements and the flow rate of the continuous phase. Hence, the d_{32} of the bubble diameter can be expressed as:

$$\frac{d_{32}}{D_0}=k\times We^{m}\times \tau^{s} \tag{3}$$

where, m=−0.35, and k and s are constants; $\tau=t_m/t^*$, $t_m=NL_E/u$ is the residence time, N is the number of mixing groups, and L_E stands for the length of a single mixing group; $t^*=D_0^2/v_G$ is the characteristic time, v_G is kinematic viscosity of the gas phase under the current experimental conditions. Eq. (3) can be expressed in logarithmic form:

$$\log_{10}\left(\frac{d_{32}}{D_0}We^{-m}\right)=\log_{10}(k)+\log_{10}(\tau) \tag{4}$$

By this form, the relationship of Eq. (3) can be converted into the relationship between $d_{32}/D_0\times We^{-m}$ and τ in Eq. (4). The relationship between all the dimensionless diameters of bubble groups for various phase flow rates of water can be linearly fitted using least square method as shown in Fig. 10. That is, the d_{32} of the bubble groups is related to Eq. (4), regardless of the liquid phase flow rate, where $\log_{10}(k)$ is the intercept of the fitted line and s is the slope. The slope of the regression line in Fig. 10 is s=−0.17 and k=0.026. Then, Equation 4 can be written as:

$$\frac{d_{32}}{D_0}=0.026\times We^{-0.35}\times \tau^{-0.17} \tag{5}$$

The deviation profiles about dimensionless $(d_{32}/D_0)\times We^{0.35}$ and dimensionless residence time between Eq. (5) and the experiment results are depicted as shown in Fig. 10. The empirical relationship with a smaller deviation range of −8.74%~+6.96% could be used to predict the bubble characteristics of TKSM with higher continuous phase and lower gas fraction than 7.41%.

CONCLUSIONS

The bubble flow characteristics of gas-liquid two-phase mixing process in a static mixer with three twisted leaves (TKSM) were experimentally studied under the liquid Re=9,836-56,206 with average gas fractions α=4.76%-66.67% at the inlet. The flow pattern in the TKSM was still in bubbly flow at lower flow rate of continuous phase $Q_L\leq 1.0$ m^3/h and the gas fraction α=54.55%-66.67%.

The bubble diameter decreased gradually with the increase of

both the number of mixing elements and liquid volume flux at the same air flow rate. The bubble diameter decreased at a faster rate in the first two groups of mixing elements and linearly decreased at a slower rate in the other mixing groups. As the number of mixing groups increased, the peak not only moved toward the smaller diameter but also became much larger and narrower. The diameter of bubble groups exhibited a Gaussian distribution with long tails of larger bubbles. The local minimum of d_{32} was obtained at Q_L=0.60 m^3/h and Q_G=0.72 m^3/h and the probability of bubble diameter d_B/D_0 less than 0.02 is 13.67% and 84.50% of the d_B/D_0 was in the range of 0.02-0.05. A general correlation among the dimensionless Sauter mean diameter d_{32}, liquid phase We and the non-dimensional residence time τ was obtained as $We^{0.35}\cdot d_{32}/D_0 = 0.026\tau^{-0.17}$.

ACKNOWLEDGEMENTS

The authors acknowledge funding support for this research from the Shenyang Science and Technology Project (RC180011, RC200032), National Natural Science Foundation of China (21476142), Liaoning Provincial Department of Education Research Project Plan (LQ2019003), Project of Liaoning Distinguished Professor Program (LCH [2018] No. 35), the Science and Technology Research Project of Liaoning BaiQianWan Talents Program (201892151), and Liaoning Natural Science Foundation Project (2019-ZD-0082).

NOMENCLATURE

MW : measurement window
d_B : diameter of the single bubble [mm]
d_{32} : sauter mean diameter [mm]
D_0 : inner diameter of the mixer [mm]
G : mass flow rate [kg/m^2s]
n : total number of bubbles in a mixing segment
n_i : numbers of bubbles with the same diameter
N : total number of mixing element
Q_G : flow rate of gas phase [m^3/h]
Q_L : flow rate of liquid phase [m^3/h]
Re : Reynolds number
t_m : residence time [s]
u : velocity of continuous phase [m/s]
We : Weber number

Greek Letter

α : gas fraction
ρ : density [kg/m^3]
σ : surface tension [N/m]
τ : non-dimensional residence time

REFERENCES

1. L. X. Zhou, *Int. J. Multiphas. Flow*, **36**, 100 (2010).
2. G. Tryggvason, S. Dabiri, B. Aboulhasanzadeh and J. Lu, *Phys. Fluids*, **25**, 031302 (2013).
3. E. A. Mansur, M. X. Ye, Y. D. Wang and Y. Y. Dai, *Chin. J. Chem. Eng.*, **16**, 503 (2008).
4. A. Bertsch, S. Heimgartner, P. Cousseau and P. Renaud, *Lab. Chip.*, **1**, 56 (2001).
5. A. Ghanem, T. Lemenand, D. Della Valle and H. Peerhossaini, *Chem. Eng. Res. Des.*, **92**, 205 (2014).
6. T. Bayer and K. Himmler, *Chem. Eng. Technol.*, **28**, 285 (2005).
7. R. K. Thakur, C. H. Vial, K. D. P. Nigam, E. B. Nauman and G. Djelveh, *Trans. Inst. Chem. Eng.*, **81**, 787 (2003).
8. D. M. Hobbs and F. Z. Muzzio, *Chem. Eng. J.*, **70**, 93 (1998).
9. D. M. Hobbs, M. M. Alvarez and F. Z. Muzzio, *Fractals*, **5**, 395 (1997).
10. D. M. Hobbs and F. Z. Muzzio, *AIChE J.*, **43**, 3121 (1997).
11. D. M. Hobbs and F. Z. Muzzio, *Chem. Eng. Sci.*, **53**, 3199 (1998).
12. V. Kumar, V. Shirke and K. D. P. Nigam, *Chem. Eng. J.*, **139**, 284 (2008).
13. F. Zidouni, E. Krepper, R. Rzehak, S. Rabha, M. Schubert and U. Hampel, *Chem. Eng. Sci.*, **137**, 476 (2015).
14. M. M. Haddadi, S. H. Hosseini, D. Rashtchian and G. Ahmadi, *Chin. J. Chem. Eng.*, **28**, 348 (2020).
15. H. Tajima, A. Yamasaki, F. Kiyono and H. Teng, *AIChE J.*, **50**, 871 (2004).
16. H. Tajima, A. Yamasaki, F. Kiyono and H. Teng, *AIChE J.*, **52**, 2991 (2006).
17. H. Tajima, R. Nagaosa, A. Yamasaki and F. Kiyono, *AIChE J.*, **56**, 2706 (2010).
18. J. H. Wu, Chinese Patent, 200,510,045,606.8 (2007).
19. J. Zhang, T. X. Kang, B. Gong and J. H. Wu, *CIESC J.*, **62**, 52 (2011).
20. H. B. Meng, F. Wang, Y. F. Yu, M. Y. Song and J. H. Wu, *Ind. Eng. Chem. Res.*, **53**, 4084 (2014).
21. M. Liu, *Ind. Eng. Chem. Res.*, **51**, 7081 (2012).
22. H. S. Song and S. P. Han, *Chem. Eng. Sci.*, **60**, 5696 (2005).
23. Z. Jaworski, P. Pianko-Opyrch, D. L. Marchisio and A. W. Nienow, *Chem. Eng. Res. Des.*, **85**, 753 (2007).
24. H. B. Meng, Y. F. Yu, Z. Q. Liu and J. H. Wu, *J. B. Univ. Chem. Technol. (Nat Sci Ed)*, **36**, 97 (2009).
25. M. X. Yue, F. Xie, J. Zhang, Q. Yuan and L. Zhang, *J. Exp. Flu. Mech. (China)*, **29**, 87 (2015).
26. L. X. Cheng, G. Ribatski and J. R. Thome, *Appl. Mech. Rev.*, **61**, 050802-1 (2008).
27. H. H. Zhang and T. F. Wang, *CIESC J.*, **70**, 487 (2019).